Int J Adv Manuf Technol (2016) 85:2377–2388
DOI 10.1007/s00170-015-8077-z

ORIGINAL ARTICLE

Finite element simulation for Ti-6Al-4V alloy deformation near the exit of orthogonal cutting

Jiapeng Lu [1,2] · Jianbin Chen [1,2] · Qihong Fang [1,2,3] · Bin Liu [4] · Youwen Liu [1,2] · Tan Jin [2,3]

Received: 4 June 2015 / Accepted: 3 November 2015 / Published online: 17 November 2015

Abstract Ti-6Al-4V alloy is known as a typical difficult-to-machine hard material due to its inherent properties such as low thermal conductivity, low elastic modulus, and high reactivity with cutting tool materials. This paper proposes a two-dimensional coupled thermo-mechanical model of plane strain orthogonal cutting for Ti-6Al-4V alloy deformation near the exit edge. Johnson–Cook material constitutive model and Cockroft–Latham damage criterion are utilized in the model for better understanding the plastic behavior and chips formation during the cutting process. The machining parameters such as cutting speed, tool edge radius, rake angle, and cutting depth are taken into account in the simulation. The results show that an edge defect generates at the exit edge after machining. The edge defect consists of two fracture surfaces, namely, the first fracture surface of opening-mode crack and the second fracture surface of sliding-mode crack. Besides, the edge defect sizes are greatly sensitive to machining parameters. This study provides a better understanding of burr/breakout formation mechanism near the exit surface and optimization of machining parameters in cutting Ti-6Al-4V alloy.

✉ Qihong Fang
fangqh1327@hnu.edu.cn

[1] State Key Laboratory of Advanced Design and Manufacturing for Vehicle Body, Hunan University, Changsha 410082, People's Republic of China

[2] College of Mechanical and Vehicle Engineering, Hunan University, Changsha 410082, People's Republic of China

[3] National Research Centre for High Efficiency Grinding, Hunan University, Changsha 410082, People's Republic of China

[4] State Key Laboratory for Powder Metallurgy, Central South University, Changsha 410082, People's Republic of China

Keywords Ti-6Al-4V alloy · Edge defect · Orthogonal cutting · Burr · FEM

1 Introduction

There are always burrs or breakouts on the exit edges of parts after machining, which cannot be prevented [1] and may result in a number of problems. On one hand, the real geometry of the workpiece edges is determined by the formation of burrs near the exit edges in the final manufacturing process. On the other hand, burrs which initially stick to a part can become loose during operation of a product and cause damage later on [2]. Thus, deburring is a necessary part of the production process in order to ensure the desired part functionality. However, burr removal is usually time-consuming and expensive. Studies show that it represents as much as 30 % of the cost of finished parts, most of which is caused by an increase of about 15 % in man power and cycle time. In addition, a 2 % share in the reject rate and 4 % share in machine breakdown times as is reported [2]. To decrease manufacturing costs, it is necessary to select the most desirable deburring methods, as well as to identify dominant process parameters on burr formation. Consequently, studying the burr/breakout formation mechanism and the effects of machining parameters on burr/breakout plays an important role in precision manufacturing.

Over the past decades, investigations on burr formation in typical machining modes have been carried out using all kinds of research methods. Gillespie et al. [1] presented an analytical model to predict burr properties and establish the first fundamental work dedicated to burr formation mechanism. In their study, four types of machining burrs including Poisson burr, rollover burr, tear burr, and cut-off burr were described. Among the previous literatures [3–10], burr formations in orthogonal cutting were studied analytically as the plastic

bending of non-cut parts of materials using minimum energy principles and the incompressibility assumption. Meanwhile, numbers of predictive models of burr dimension including different conditions were carried out as well. Ko and Dornfeld [3] proposed a quantitative model of burr formation for ductile materials to calculate burr height and burr thickness. In the model, the burr formation mechanism was divided into three parts: initiation, development, and formation and validated by the observation of machining copper. Based on the work of ductile materials, they further developed the quantitative model including fracture of the workpiece during burr formation and acquired a theoretical formulation of burr height and length [4]. An analytical model considering oblique cutting was also presented by Ko and Dornfeld [5] to investigate the burr formation and fracture mechanism in the realistic oblique-machining case. Chern et al. [6] studied a burr/breakout formation based on the observation of SEM micro-machining tests for orthogonal cutting. Toropov et al. [7] proposed a model including continuous burr development and discontinuous development of burr formation mechanism. The model allowed predicting burr height and thickness and was able to simulate burr development. A new model based on the theory of slip-lines was proposed by Toropov et al. [8] to predict the full formation of a burr in orthogonal cutting. Based on the geometry of burr formation and the principle of continuity of work at the transition from chip formation to burr formation, Niknam et al. [9] calculated the burr thickness in milling of ductile materials. A computational model was recently presented by Niknam and Songmene [10] to approximate the tangential cutting force and consequently predict the thickness of the exit up milling side burr. In addition, since burr/breakout formation is a complex process and difficult to observe by experiment, the finite element simulation is widely used in engineering to analyze the burr formation mechanism [11–13]. Finite element models in orthogonal cutting were presented by Park et al. [12] to examine the influences of exit angles of the workpiece, tool rake angles, and backup materials on burr formation process in cutting 304 L strainless steel. Deng et al. [13] investigated the effect of the tool conditions and cutting conditions on the burr formation process based on a coupled thermo-mechanical model of plane strain orthogonal metal cutting. Except for the burr formations of ductile materials near the final manufacturing process, investigations of burr formation in machining brittle materials have also been carried out in various research methods. Cao [14] proposed a finite element analysis based on the theory of fracture mechanics to investigate the size of exit edge chipping in ceramic machining. According to the orthogonal cutting model of SiCp/Al composites, Zhou et al. [15, 16] analyzed the influences of cutting velocity, cutting depth, and tool rake angle on the cutting force and edge defects near the exit of orthogonal cutting. Besides, Zhou et al. [17–19] have done a great deal of successful works on the interaction between material defects and cracks which may have potentially significant application in addressing challenging material science, especially their wear and contact fatigue analysis.

The above review of literatures shows that the burr/breakout formation in machining ductile materials and brittle materials has been studied extensively using experimental and predictive analytical modeling, but few works related to hard materials such as Ti-6Al-4V alloy were carried out. Ti-6Al-4V alloy is an important aerospace engineering material due to its excellent combination of strength and fracture toughness as well as low density [20]. However, this material is regarded as difficult to machined material [21, 22]. Recently, Ti-6Al-4V alloy machining has been studied extensively in experimental and finite element methods, especially on machining in high-speed machining. Umbrello [23] presented a finite element analysis of machining Ti-6Al-4V alloy both for conventional and high-speed cutting regimes. In particular, chip morphology, cutting force, and segmentation were taken into consideration due to their predominant roles in determining machinability during the machining of these alloys. In addition, many finite element models of orthogonal cutting Ti-6Al-4V alloy have been carried out [24–27] for different research contents and show that work material flow, friction parameters between the tool/workpiece interface, the tool material [28], the fracture criterion, and the thermal parameters play an important role in the success and reliability of numerical models. In other words, it depends on the choice of appropriate constitutive equations.

This paper displays a two-dimensional finite element model of burr formation in machining Ti-6Al-4V alloy. The Johnson–Cook material model and Cockroft–Latham damage criterion are used for better understanding plastic flow and chips formation in the machining process. The purpose of this model is to simulate the Ti-6Al-4V alloy deformation near the exit and investigate the influences of cutting speed, rake angle, exit angle, cutting edge radius, the depth of cutting on edge defect dimensions, and profile. It is aimed to provide a fundamental understanding for the effects of machining parameters on edge defect sizes and the formation mechanism, which may provide guidance in terms of the optimization of cutting parameters design.

2 Finite element models

2.1 Boundary conditions and friction model

Figure 1a shows the boundary conditions and initial geometry configuration. The sizes of workpiece A-B-C-D-A are 1.5 × 0.8 mm in X and Y directions, and the cutting tool E-F-G-H-E is modeled as a rigid but heat transfer body. The boundary E-B-C is fixed, while the boundary C-D-A is set as free to allow the chip and burr to form without any constraint during the

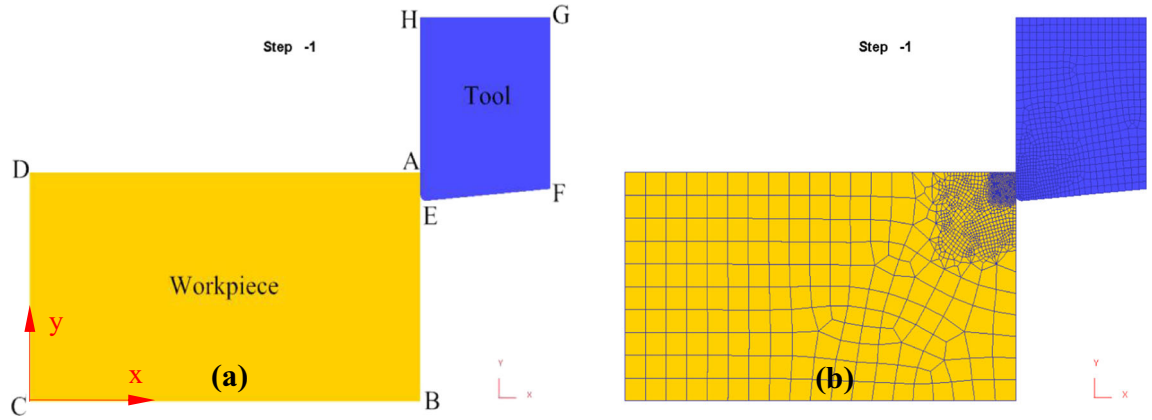

Fig. 1 Orthogonal cutting model. **a** Tool and workpiece. **b** Meshed tool and workpiece

simulation. In addition, heat exchange with environment is allowed on the boundary C-D-A and F-G-H, and the environment temperature is set as 20 °C. Due to the complex condition, the contact between tool and workpiece is defined as rigid and flexible, meanwhile self-contact between workpiece and chip is also taken into account [29]. The heat-transfer coefficient among all the contact zone is 45 N/s/mm/°C. In addition, the contact faces around the tool are divided into two friction windows during the movement. The one near the tool is called bonded friction zone; the other is named as slip friction zone. The friction boundary condition can be expressed as follows [30]:

$$T_f = \begin{cases} \mu\sigma_n & (T_f < T_{\max}) \\ T_{\max} & (T_f \geq T_{\max}) \end{cases} \quad (1)$$

where T_f is the friction stress, μ is the Coulomb friction coefficient, σ_n the normal stress, and $T_{\max}$ the critical shear yield stress. Besides, for the heat transfer calculation, the following assumptions are made:

1. The main heating sources during Ti-6Al-4V alloy cutting are the plastic deformation zone and the friction at the tool/workpiece interface [13].
2. The tool-chip contact is thermally perfect, namely, a significantly large value for the interface heat transfer coefficient is taken. The boundary B-C and H-G-F that are away from the cutting zone remain room temperature 20 °C.
3. For the free surfaces on the workpiece, tool, and chip, heat loss by convection and radiation is considered to be insignificant. Therefore, it can be negligible [31].

Figure 1b shows the initial meshing of the tool and workpiece. Based on the updated Lagrangian formulation for large plastic deformation analysis, the workpiece is divided into 8564 elements considering plane strain assumption, and in addition, the mesh of severe deformation zone is refined for improving efficiency and precision. The chip formation process is simulated as plastic flow and the chip separation from the workpiece is achieved by continuous re-meshing. After each re-meshing step, the solutions of the process state variables for the workpiece is then interpolated from the original mesh to the current undeformed mesh [31].

2.2 Material modeling

Titanium and its alloys are used widely in aerospace, pressure vessels, aircraft turbine and compressor blades and disks, and surgical implants [20]. However, many characteristics such as low elastic modulus and chemical reaction with tool materials make titanium alloys hard and expensive to machine [21, 22]. The Ti-6Al-4V alloy serves as the workpiece material in this paper and its chemical composition is given in Table 1.

Materials' properties such as Poisson ratio, density, thermal conductivity, and specific heat properties have to be provided as input to the finite element simulation accurately; otherwise, the simulation results would be unreliable [24]. In this study, WC alloy is chosen as the tool material, the thermal conductivity is 59 W/m·K, heat capacity 15 J/kg·K, and density 14.5×10^3 kg/m^3. The mechanical and physical properties of Ti-6Al-4V alloy are presented in Table 2.

In high speed metal cutting and forming process, the workpiece material undergoes plastic deformation over wide ranges of strain, strain rate, and temperature [32–34]. The process is governed by different deformation mechanisms depending on the above parameters as well as their variation during the process [35]. In the severe deformation zone ahead of the tool tip, the local strain can increase from nil to very high value within a short time. The local strain rate varies between 0 and 5×10^4 s^{-1}. The deformation work is transferred into heat during the cutting. Then the local temperature can increase to the values slightly below melting point [36]. To model the plastic behavior of Ti-6Al-4V alloy during the cutting process, the Johnson–Cook material constitutive model [37] is employed. The strain rate-dependent hardening and temperature-dependent flow softening behavior on the plastic deformation

Table 1 Chemical composition of Ti-6Al-4V alloy [20]

Element	Ti	Al	V	Fe/O
Component (wt.%)	90	6	4	Max 0.2

Table 3 The J-C equation parameters of Ti-6Al-4V alloy [23]

I (MPa)	*J* (MPa)	*K*	*n*	*m*
870	990	0.008	1.01	1

are incorporated in the model as multiplication form [38]. The J-C constitutive equation including five parameters can be described as follows:

$$\sigma = \left(I + J\varepsilon^{n}\right)\left(1 + K\ln\dot{\varepsilon}\right)\left[1-\left(T^{*}\right)^{m}\right] \quad (2)$$

where I, J, and n are the three coefficients describing the quasi-static behavior of material, while K and m account for the strain rate hardening and thermal softening effects, respectively; $\dot{\varepsilon}$ is the reference strain rate, T^{*} is the homologous temperature and can be further defined by:

$$T^{*} = (T-T_r)/(T_m-T_r) \quad (3)$$

where T is the absolute temperature , T_r and T_m represent the room and melting absolute temperatures, respectively. And the five parameters are shown in Table 3.

2.3 Material damage criterion

In order to calculate the formability limit of Ti-6Al-4V alloy, ductile fracture criteria have to be defined. Takuda [39] have proved that the combination of the finite element simulation and the ductile fracture criteria is convincing in the prediction of forming limit. Among the various fracture proposed, the criterion suggested by Cockroft and Latham is found to predict the most reasonable fracture strain in metal forming operations [40]. In this research, Cockcroft and Latham's criterion [41] is employed to predict the effect of tensile stress on the edge defect formation near the exit of orthogonal cutting. According to the fracture strain energy, Cockcroft and Latham's criterion can be expressed as follows:

$$\int_0^{\varepsilon_f} \sigma_1 d\bar{\varepsilon} = R \quad (4)$$

Table 2 Mechanical and physical properties of Ti-6Al-4V alloy [25]

Density (kg/m^3)	4.43×10^3
Ultimate tensile strength (MPa)	950
Tensile yield strength (MPa)	880
Modulus of elasticity (GPa)	113.8
Thermal conductivity (W/m·*K*)	17
Poisson's ratio	0.342
Heat capacity (J/kg·*K*)	526

where ε_f is the effective strain, σ_1 is the maximum principal stress, and R is a material constant. Cockcroft and Latham's criterion means that when the integral of the largest tensile principal stress component over the plastic strain reaches the critical value R, which is called damage value, fracture occurs or chip segmentation starts.

In FE simulation, the critical damage value of each element is calculated under deformation at each time step by the program. Once the damage value in an element reaches a critical one, cracks initiate, and these elements will be deleted, and then the rough boundary produced by the element deletion is smoothed by element re-meshing [23]. In this paper, the critical damage value of Cockcroft and Latham's criteria is set as 240.

3 Results and discussion

3.1 The machining process

Ti-6Al-4V alloy machining essentially is a highly nonlinear and coupled thermo-mechanical process, during which the workpiece material ahead of the tool tip undergoes large deformation, high strain rate, high temperature, and complex friction. In Fig. 2, the coupled thermo-mechanical effect is investigated during chips formation near the exit edge under cutting speed v=800 mm/s, cutting depth a_p=0.1 mm, and the cutting tool edge radius r=0.02 mm. The results presented in Fig. 2 show the effective stress contours in different stages during the cutting process. In particular, the case in which the tool exits is analyzed in detail for better understanding the burr/breakout formation. Figure 2a shows the initial contact stage when the tool cuts into the workpiece. In this case, the magnitude of effective stress ahead of the tool tip reveals the severe shearing zone of the workpiece material [13]. Figure 2b presents the steady state of chip formation. In this stage, due to adiabatic shear bands and crack propagation, the chip morphology is generated with continuous saw-toothed [26]. Besides, the cutting force and cutting temperature reach approximately the steady state. Figure 2c displays the continuous cutting state. The deformation and stress distribution are not affected by the workpiece edge. As the tool advances toward the workpiece edge, the plastic deformation zone around the primary shear zone is accompanied to extend accordingly. Figure 2d shows crack initiation stage. The plastic deformation zone around the primary shear zone extends to the workpiece edge and turns into negative shear band. As the

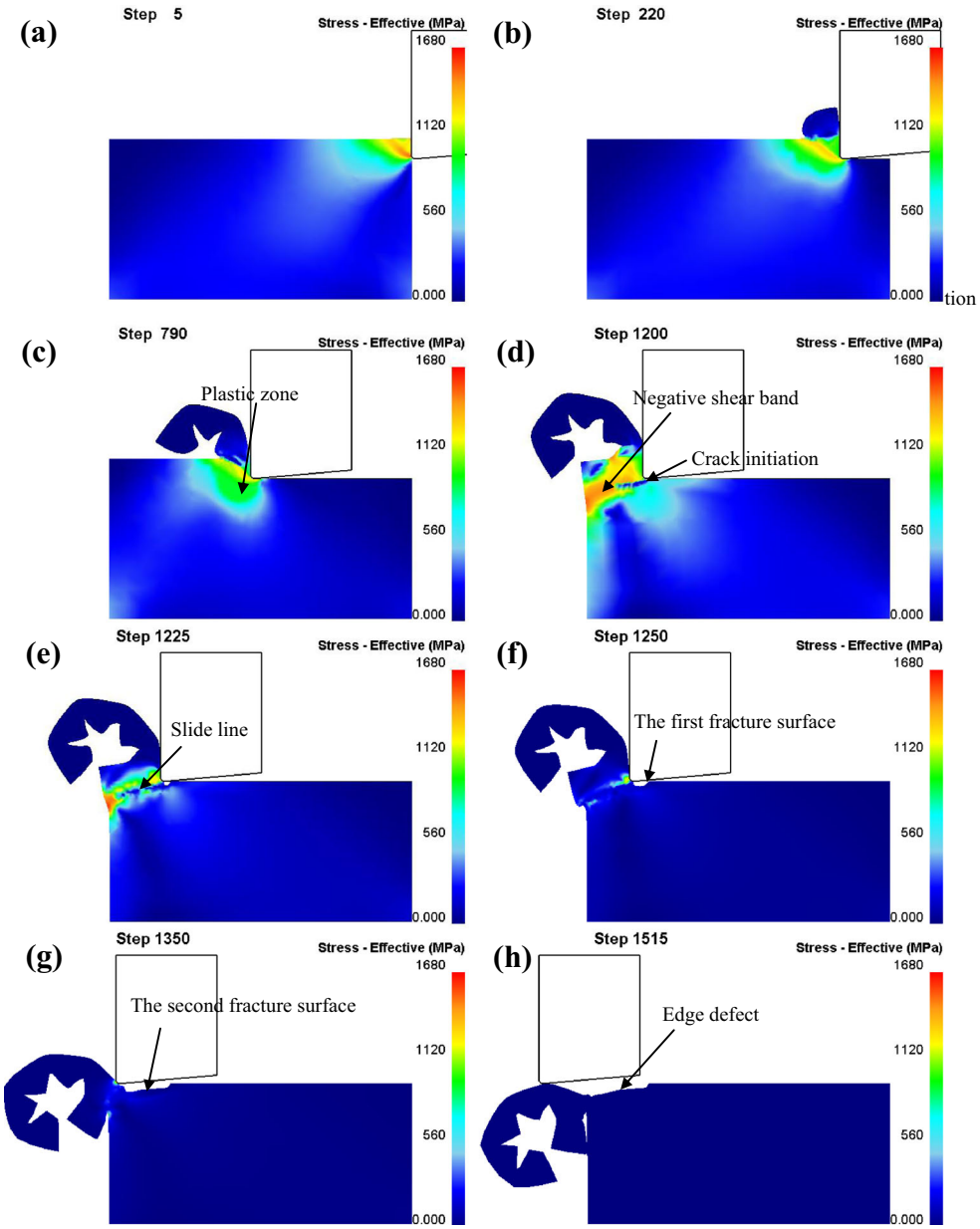

Fig. 2 **a**–**h** Formation process of the edge defect during Ti-6Al-4V alloy cutting

tool moves toward the workpiece edge, an opening-mode crack initiates at tool tip. Figure 2e reveals crack propagation stage. In this stage, the chip formation is considered to be stop while the left corner region of the workpiece remains undeformed. With the above region rotating around the plastic hinge point, the crack propagates along the direction vertical to the finished surface and turns into the first fracture surface of opening-mode crack. In this simulation, it is assumed that as soon as four neighboring elements reach the critical damage value 240, the material is then ready to fracture and those elements are then removed [13]. In addition, it is noted that the zone of effective stress bigger than 560 Mpa starts decreasing, which indicates the cutting forces start decreasing due to the rotation of undeformed chip layer. Figure 2f describes the second crack initiation stage. The crack does not continue to spread along the direction vertical to finished surface but along the direction of negative shear band. Figure 2g indicates the sliding stage. As the tool approaches the end of the workpiece, the left corner region of the workpiece does not rotate around the plastic hinge point as the ductile material [13], but slides along the direction of negative shear band. And then a fracture surface of sliding-mode crack is generated. Figure 2h shows eventually the tool cuts through the workpiece. The crack makes the chip separate along the sliding line. Eventually, the tool unloads and cutting is finished as soon as contact is lost with the workpiece, an area consisting of two fracture

surfaces is the edge defect produced which possesses a certain height and width.

3.2 The cutting velocity

Figure 3 shows the effective strain plots of the exit edge defect generated during orthogonal cutting Ti-6Al-4V alloy under four different cutting velocities. It can be observed that the effective strain distribution, the chip morphology and the edge defect morphology are greatly different under various speeds. In Fig. 3a, when the cutting velocity v=200 mm/s, the maximum effective strain is 4.773 and located in the sliding line, which indicates that the left corner region of workpiece slides along the direction of negative shear band. And the produced fracture surface of sliding-mode crack is smooth and oblique. In Fig. 3b, with the increase of cutting velocity from v=200 mm/s to v=500 mm/s, the maximum effective stress increases to 5.518 significantly, which reveals the severer sliding deformation. In addition, it can be noted that the edge defects are obviously consisted of two fracture surfaces. One is the surface located in crack initial position, which is very steep and even vertical to finished surface. This fracture surface can be explained by the findings of Velásquez et al. [42]; it is found that there is no phase transformation in the near-surface region during Ti-6Al-4V alloy machining, and the subsurface is only affected by plastic deformation. Work hardening of the deformed layer beneath the machined surface up to 0.01 mm causes higher hardness than the average hardness of the base material [22, 43]. This indicates that a plastic hardening layer generates near the machined surface [44]. According to the minimum energy principle, the first fracture surface perpendicular to the finished surface can be explained by that the crack propagation along the direction vertical to the hardening layer needs the minimum energy. In order to the convenience of description, we call it the first fracture surface. Compared with machining ductile and brittle materials formation near the exit of orthogonal cutting [13, 15, 16], it can be seen that the first fracture surface only appears in machining hard materials such as Ti-6Al-4V alloy. Another fracture surface is the surface near the exit edge. As the tool advances, the undeformed chip layer in front of the tool does not rotate around the pivoting point as ductile materials [13] but slides along the slide line, and then the second fracture surface of sliding-mode crack is formed. It can be observed that the second fracture surface is a smooth surface and has a bigger area than the first one. As the cutting velocity v=800 mm/s shown as Fig. 3d, it is seen that the boundary between the first fracture surface and the second fracture surface becomes clearer. In metal machining, according to the work of Chou and Evans [45], the affected layer depth $\frac{2z_{cr}}{VB}$ is a function of cutting speed $\frac{2z_{cr}}{VB} = f\ (L, v)$. And the plastic hardening layer thickness increases with the cutting speed [42]; the size of the first fracture surface is proportional to the thickness of plastic hardening layer. As a result, the first fracture surface is steeper and longer with the increasing cutting speed.

Figure 4 shows the influence of cutting velocity on the edge defect sizes. Compared with the edge defects in machining brittle materials [14–16], it can be

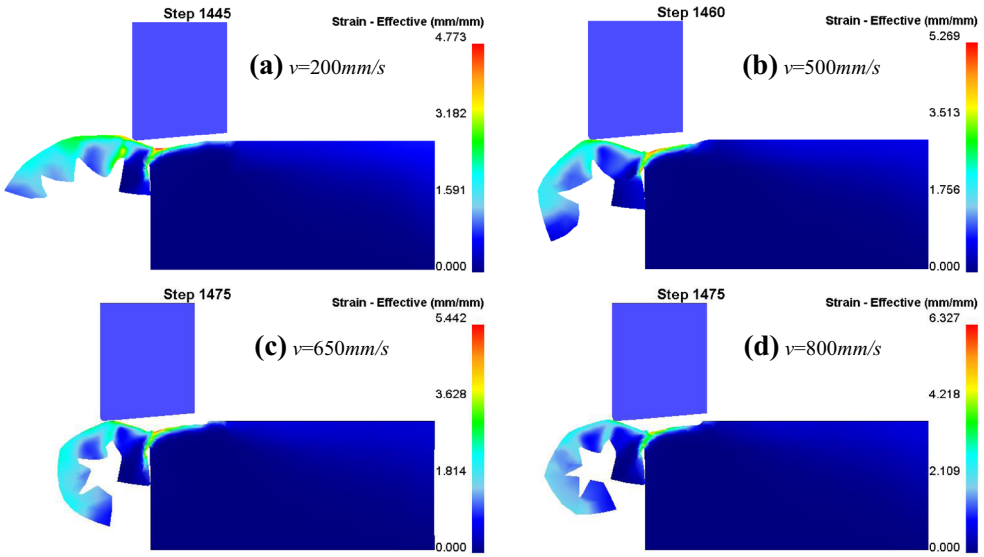

Fig. 3 **a**–**d** The influence of cutting velocity on burr formation (a_p=0.1 mm, α=0°, r=0.02 mm)

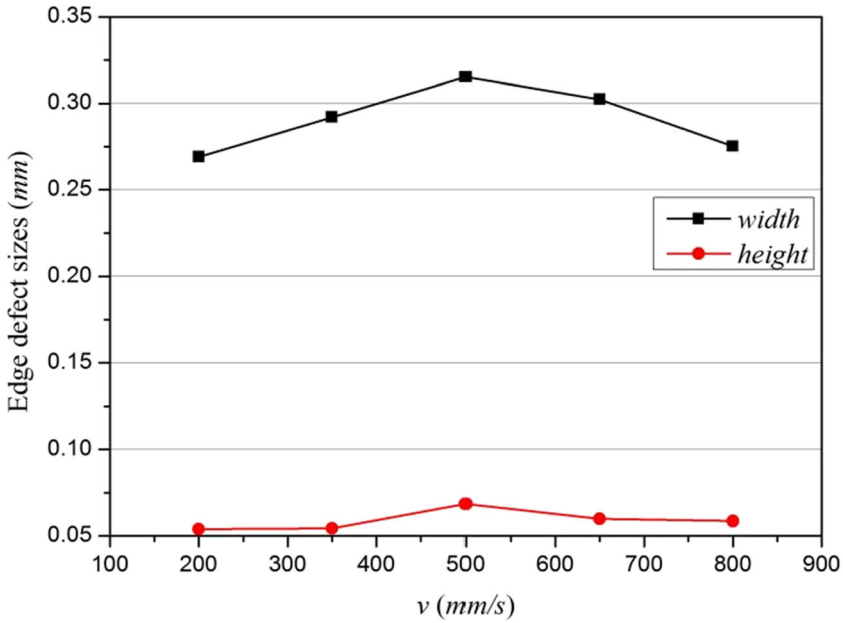

Fig. 4 The influence of cutting velocity on edge defect sizes

observed that the ratio between the height and the width is very small in machining Ti-6Al-4V alloy. The average ratio is r_0=0.203 in this research, while r_0=1.05 in orthogonal cutting SiCp/Al composites [15, 16]. The reason is that the plastic deformation in the fracture surface absorbs part of the energy form the crack propagation, and according to the minimum energy principle, the sliding-mode crack extends along edge of plastic deformation zone. Based on the J-C constitutive model of Ti-6Al-4V alloy, the strain rate and temperature are the two obvious effects on the plastic deformation behavior, and flow stress decreases markedly with temperature at a fixed strain rate but increases with strain rate for a given temperature [46]. This indicates the strain rate and temperature lead to work hardening and softening, respectively. When cutting velocity within the low value range, the strain rate is small and cannot give rise to apparent material hardening effect. However, the temperature increases sharply resulting in material softening behavior. Consequently, as the cutting velocity increases both of the height and width increase within the low velocity range. And the width of edge defect is more sensitive to cutting velocity. When the cutting velocity ascends to the critical value v=500 mm/s, the sizes of edge defects reach the maximum. However, the sizes of edge defects decrease in the velocity range larger than v=500 mm/s with the increasing cutting velocity. This can be explained by that the high strain rate at higher speed cutting causes strain hardening and generates a plastic hardening layer at subsurface. Thus, the edge defects decrease as the cutting velocity increases. As a result, from the viewpoint of edge defect minimization and efficient machining, a higher cutting velocity should be chosen for Ti-6Al-4V alloy machining near the exit edge.

3.3 The cutting edge radius

Figure 5 presents the influence of the cutting edge radius on the edge defect sizes and morphology under different cutting edge radii. The cutting edge radius plays an important role in orthogonal cutting since it determines the cutting edge contact length. As a result, the process variables such as contact stress, temperature field, and cutting forces are greatly different with diverse cutting radii. In Fig. 5, the maximum effective strains are 4.09, 5.018, and 5.131 under the cutting edge radius of 0, 0.02, and 0.04 mm, respectively. This indicates that the effective strain increases with increasing edge radius [30]. In addition, it can be seen that the influence of the cutting edge geometry on the edge defect profile is obvious. With the increase of the cutting edge radius, the first fracture surface of opening-mode crack becomes bigger and the boundary between the first fracture surface and the second fracture surface is clearer. This can be explained by the findings of Yen [31]; on one hand, the degree of plastic deformation in the secondary shear zone and on the machined surface increases considerably as the edge radius increases, the thickness of work hardening layer becomes bigger. On the other hand, the increased contact area around the tool tip results in the increase of the specific cutting energy as well as cutting forces. As a result, the crack propagates deeper and steeper at the same strain rate and temperature.

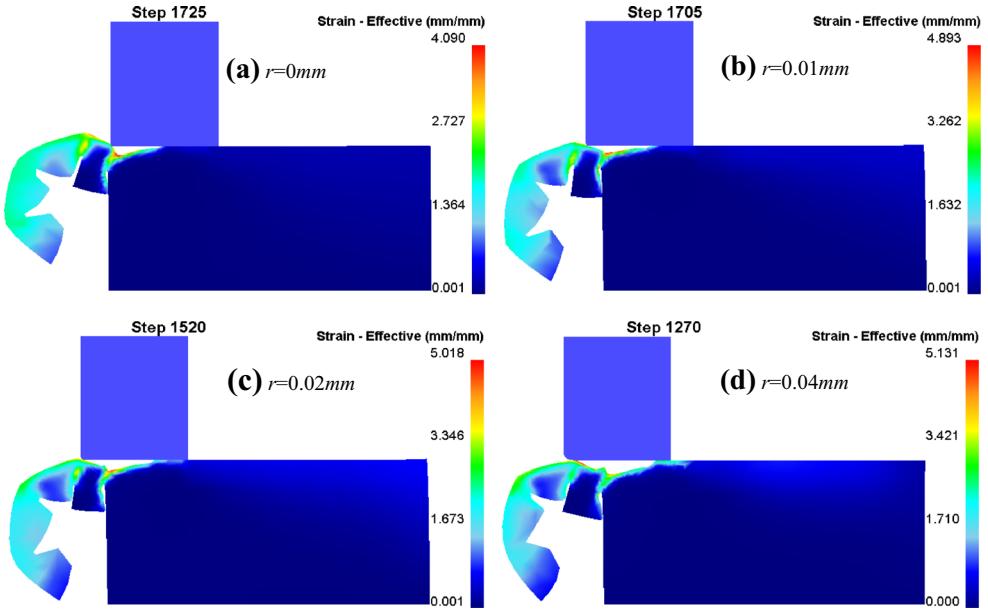

Fig. 5 **a**–**d** The effect of cutting radius on burr formation (v=500 mm/s, a_p=0.1 mm, α=0°)

Figure 6 shows that the relationship between the cutting edge radii and the edge defect sizes in machining Ti-6Al-4V alloy. It can be seen that with the increase of the cutting radius the height of the edge defect becomes bigger. However, the width of the edge defect is little sensitive to the cutting edge radius. The reason is that a bigger tool edge radius corresponds to a bigger Y-direction component of cutting forces and leads to the increasing height of edge defects. Therefore, in order to acquire a minimum edge defect, the tool with small edge radius should be chosen.

3.4 The rake angle

Figure 7 represents the influence of the rake angles on the edge defect under different rake angles. The rake angle always has great relationship with the tool-chip contact, and the component of cutting forces, thus, play

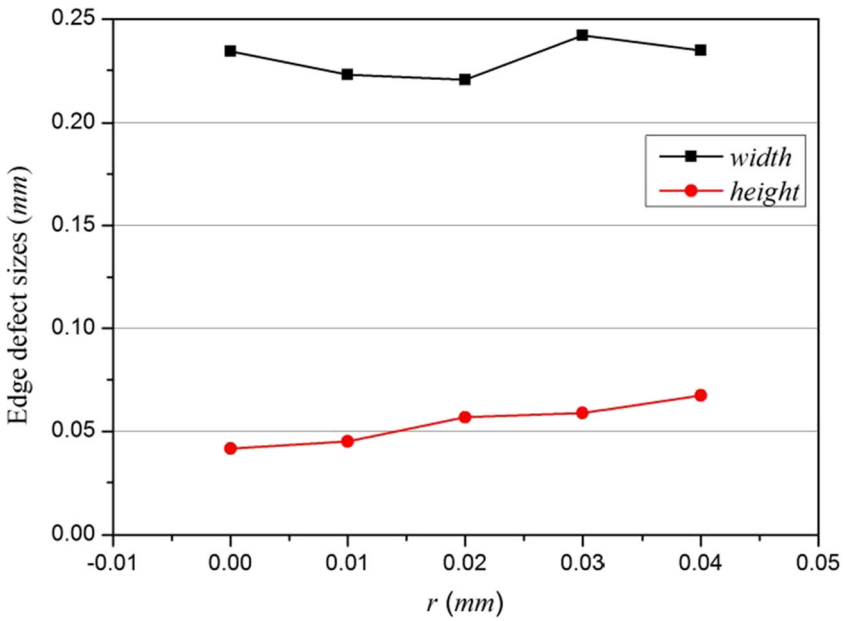

Fig. 6 The effect of the cutting edge radius on edge defect sizes

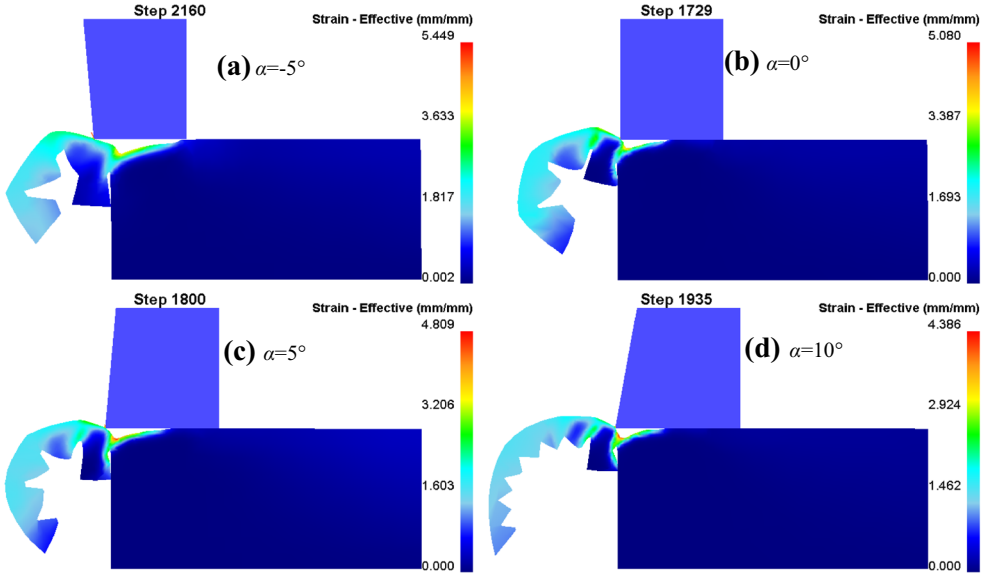

Fig. 7 **a**–**d** The influence of rake angle on burr formation (v=500 mm/s, a_p=0.1 mm, r=0 mm)

an important role to process variables. From the effective strain plots of the edge defect shown in Fig. 7, it is clear that the rake angle has a significant effect on the chip thickness, as the augment of rake angle the less material are removed, resulting in the decline of cutting forces. As a result, the maximum effective strain 5.449, 5.08, 4.809, and 4.386 shown in Fig. 7 tends to decrease with the increasing rake angle. In addition, it can be seen that the fracture surface morphology are not sensitive to the rake angles due to the rake angle has little effect on the plastic hardening layer at subsurface after machining. The first fracture surface is small and the boundary between the first fracture and the second fracture is not obvious due to the tiny hardening layer. However, the edge defect sizes shown in Fig. 8 are greatly sensitive to the rake angles. It can be observed that the lower the rake angle becomes, the earlier the transformation point of chips formation appears due to the bigger Y-direction component of cutting forces. Consequently, with the increasing of the rake angle, both the height and width of edge defect decrease.

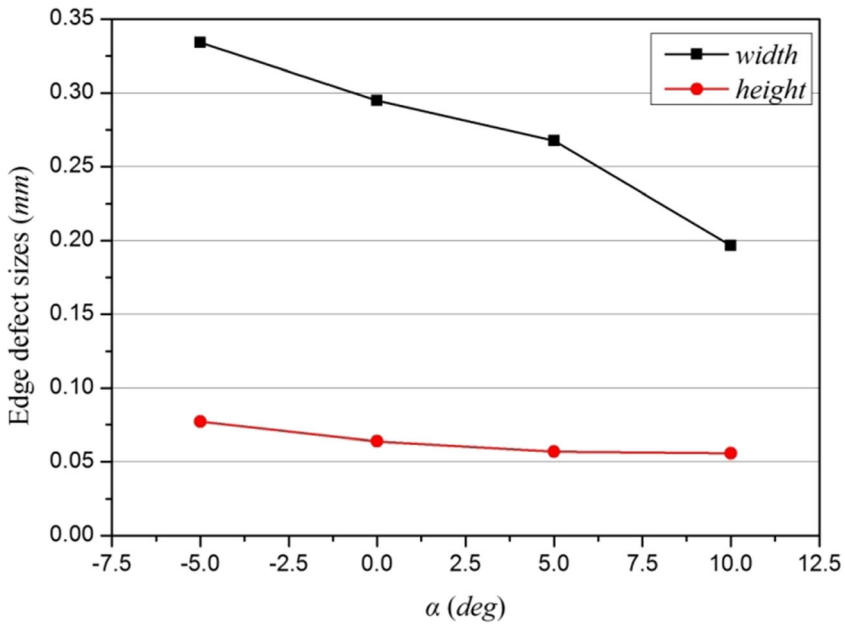

Fig. 8 The effect of rake angle on edge defect sizes

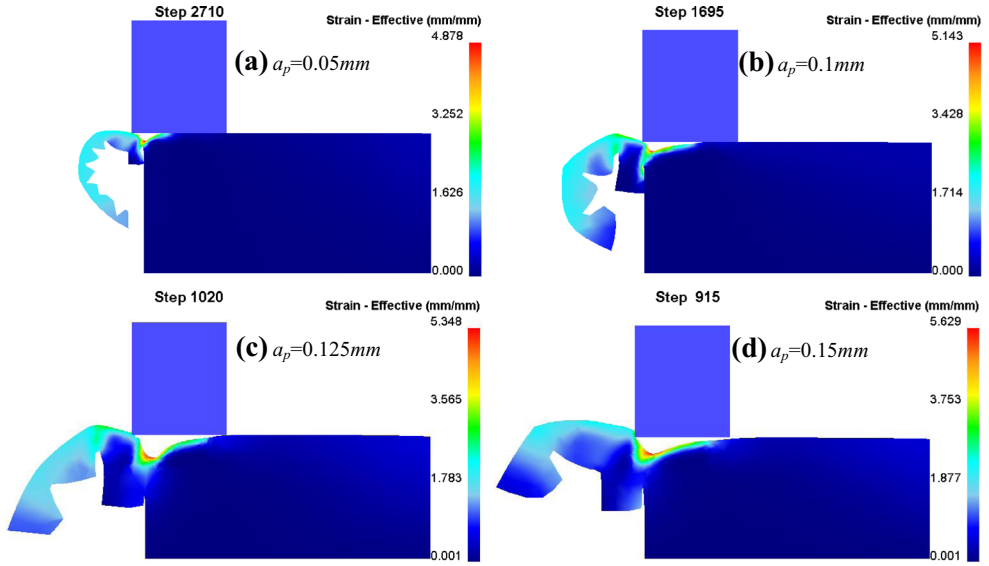

Fig. 9 **a**–**d** The effect of the depth of cutting on burr formation (v=500 mm/s, α=0°, r=0 mm)

From the viewpoint of precision machining, a bigger rake angle should be chosen for machining Ti-6Al-4V alloy near the exit surface.

3.5 The depth of cutting

Figure 9 shows the influence of the cutting depth on the edge defect sizes and morphology near the exit of orthogonal cutting Ti-6Al-4V alloy. It can be observed that the fracture surface grows as a smooth arch, and the first fracture surface is not obvious; this reveals that the thermal softening effect is greater than the work hardening with the increasing cutting depth, and the material near the finished surface becomes softened [27]. Furthermore, it is seen that the deeper cutting depth, the earlier the transition point appears. Consequently, as shown in Fig. 10, with the increase of cutting depth, both the height and width of edge defect increase and the dependence of exit edge defect sizes on cutting depth appears to be in linear relationship. This result can be explained as follows: on one hand, with the increasing of cutting depth, the bigger cutting force causes the cutting action tending to be more unstable during machining, which increases the exit edge

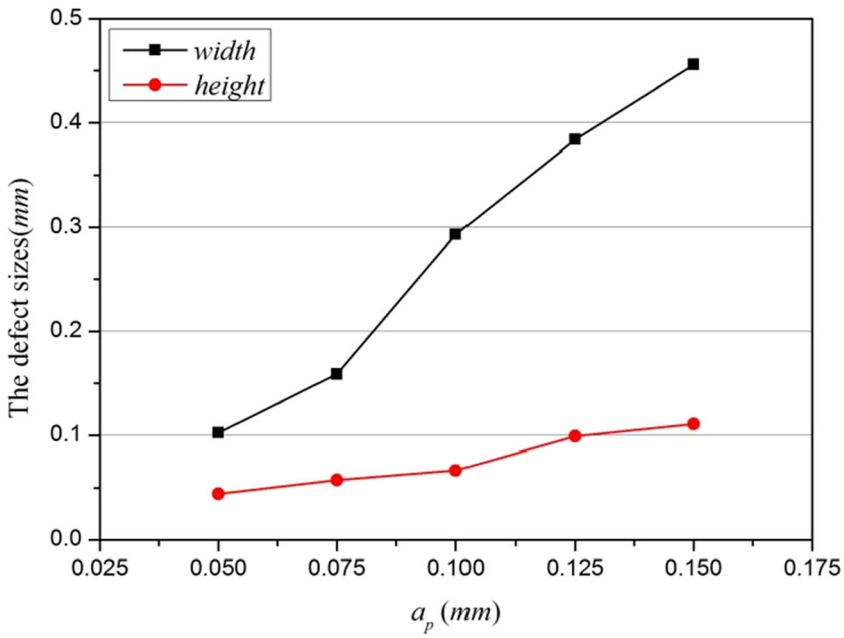

Fig. 10 The effect of cutting depth on the edge defect sizes

defect size [15]. The results are well in accordance with that of SiC/Al composite [15]. On the other hand, the cutting depth is proportional to temperature field and softening effect; as a result, the bigger cutting depth, the more material becomes softened. Therefore, from the viewpoint of exit edge defect minimization, the machining parameters with a large cutting depth should be avoided.

4 Conclusions

A more realistic finite element model of Ti-6Al-4V alloy cutting including exit edge defect formation has been proposed. The simulation procedure based on Johnson–Cook material model and Cockroft–Latham damage criterion is presented for the purpose of better understanding the exit edge deformation in cutting hard material as Ti-6Al-4V alloy and obtaining a quantitative analysis of the edge defects. The major conclusions drawn from this study are the following:

1. The edge defects generated by orthogonal cutting Ti-6Al-4V alloy near the exit consist of two fracture surfaces. The first fracture surface of opening-mode crack has a considerably small size due to the thin plastic hardening layer at subsurface and vertical to finished surface. While the second fracture surface of sliding-mode crack is flat in the position and long in the dimension.
2. The ratio r_0=0.203 between the height and width of edge defects in machining hard materials such as Ti-6Al-4V alloy is significantly small compared with that r_0=1.05 of brittle materials, since the plastic behavior in Ti-6Al-4V alloy absorbs part of the energy in crack propagation.
3. The edge defect sizes are greatly sensitive to the processing parameters. Consequently, the sizes of the edge defects are shown to be reduced by (a) enhancing the cutting velocity, (b) sharpening the cutting tool edge radius, (c) increasing the rake angle, and (d) decreasing the cutting depth.

Acknowledgments The authors would like to deeply appreciate the support from the NNSFC (11172094, 11372103, and 11172095), the NCET-11-0122, the Hunan Provincial Science Fund for Distinguished Young Scholars (2015JJ1006), the Fok Ying-Tong Education Foundation, China (141005), and the Interdisciplinary Research Project of Hunan University.

References

1. Gillespie LK, Blotter PT (1976) The formation and properties of machining burrs. J Manuf Sci E-T ASME 98:66–74
2. Aurich JC, Dornfeld D, Arrazola PJ (2009) Burrs—analysis, control and removal. CIRP Ann-Manuf Techn 58:519–542
3. Ko SL, Dornfeld DA (1991) A study on burr formation mechanism. J Eng Mater-T ASME 113:75–87
4. Sung-Lim K, Dornfeld DA (1996) Analysis of fracture in burr formation at the exit stage of metal cutting. J Mater Process Tech 58:189–200
5. Ko SL, Dornfeld DA (1996) Burr formation and fracture in oblique cutting. J Mater Process Tech 62:24–36
6. Chern GL, Dornfeld DA (1996) Burr/breakout model development and experimental verification. J Eng Mater-T ASME 118:201–206
7. Toropov A, Ko SL (2006) A model of burr formation in the feed direction in turning. Int J Mach Tool Manu 46:1913–1920
8. Toropov AA, Ko SL, Lee JM (2006) A new burr formation model for orthogonal cutting of ductile materials. CIRP Ann-Manuf Tech 55:55–58
9. Niknam SA, Songmene V (2013) Modeling of burr thickness in milling of ductile materials. Int J Adv Manuf Tech 66:2029–2039
10. Niknam SA, Songmene V (2014) Analytical modelling of slot milling exit burr size. Int J Adv Manuf Tech 73:421–432
11. Park IW, Dornfeld DA (2000) A study of burr formation processes using the finite element method: part I. J Eng Mater-T ASME 122: 221–228
12. Park IW, Dornfeld DA (2000) A study of burr formation processes using the finite element method: part II—the influences of exit angle, rake angle, and backup material on burr formation processes. J Eng Mater-T ASME 122:229–237
13. Deng WJ, Xia W, Tang Y (2009) Finite element simulation for burr formation near the exit of orthogonal cutting. Int J Adv Manuf Tech 43:1035–1045
14. Cao Y (2001) Failure analysis of exit edges in ceramic machining using finite element analysis. Eng Fail Anal 8:325–338
15. Zhou L, Wang Y, Ma ZY (2014) Finite element and experimental studies of the formation mechanism of edge defects during machining of SiCp/Al composites. Int J Mach Tool Manu 84:9–16
16. Zhou L, Hou N, Huang S (2014) An experimental study on formation mechanisms of edge defects in orthogonal cutting of SiCp/Al composites. Int J Adv Manuf Tech 72:1407–1414
17. Zhou K, Nazarov AA, Wu MS (2006) Continuum and atomistic studies of a disclinated crack in a bicrystalline nanowire. Phys Rev B 73:045410–1–045410–11
18. Zhou K, Wu MS, Nazarov AA (2008) Relaxation of a disclinated tricrystalline nanowire. Acta Mater 56:5828–36
19. Zhou K, Wei RB (2014) Modeling cracks and inclusions near surfaces under contact loading. Int J Mech Sci 83:163–171
20. Ezugwu EQ (1997) Titanium alloys and their machinability—a review. J Mater Process Tech 68:262–274
21. Ezugwu EO, Bonney J, Yamane Y (2003) An overview of the machinability of aeroengine alloys. J Mater Process Tech 134: 233–253
22. Che-Haron CH, Jawaid A (2005) The effect of machining on surface integrity of titanium alloy Ti–6% Al–4% V. J Mater Process Tech 166:188–192
23. Umbrello D (2008) Finite element simulation of conventional and high speed machining of Ti6Al4V alloy. J Mater Process Tech 196: 79–87
24. Yang SB, Xu J, Fu Y (2012) Finite element modeling of machining of hydrogenated Ti-6Al-4V alloy. J Mater Process Tech 59:253–262
25. Shao F, Liu Z, Wan Y (2010) Finite element simulation of machining of Ti-6Al-4V alloy with thermodynamical constitutive equation. J Mater Process Tech 49:431–440
26. Calamaz M, Coupard D, Girot F (2008) A new material model for 2D numerical simulation of serrated chip formation when machining titanium alloy Ti–6Al–4V. J Mater Process Tech 48:275–288
27. Yiğit K (2011) Temperature dependent flow softening of titanium alloy Ti6Al4V: an investigation using finite element simulation of machining. J Mater Process Tech 211:737–749
28. Ding WF, Xu JH, Shen M (2007) Development and performance of monolayer brazed CBN grinding tools. J Mater Process Tech 34: 491–495

29. Chen J, Fang Q, Zhang L (2014) Investigate on distribution and scatter of surface residual stress in ultra-high speed grinding. J Mater Process Tech 75:615–627
30. Filice L, Micari F, Rizzuti S (2007) A critical analysis on the friction modelling in orthogonal machining. J Mater Process Tech 47:709–714
31. Yen YC, Jain A, Altan T (2004) A finite element analysis of orthogonal machining using different tool edge geometries. J Mater Process Tech 146:72–81
32. Mao C, Zhou ZX, Ren YH, Zhang B (2010) Analysis and FEM simulation of temperature field in wet surface grinding. Mater Manuf Process 25:399–406
33. Mao C, Zhou ZX, Zhang J, Huang XM, Gu DY (2011) A comparative research of damaged layers formed in surface grinding and wire-electrodischarge machining. Mater Manuf Process 26:1473–1480
34. Mao C, Zhou ZX, Zhang J, Huang XM, Gu DY (2011) An experimental investigation of affected layers formed in grinding of AISI 52100 steel. Int J Adv Manuf Tech 54:515–523
35. Tian L, Fu Y, Xu JH (2015) The influence of speed on material removal mechanism in high speed grinding with single grit. Int J Mach Tool Manuf 89:192–201
36. El-Magd E, Treppman C, Korthäuer M (2006) Description of flow curves over wide ranges of strain rate and temperature. Z Met 97:1453–1459
37. Johnson GR, Cook WH (1983) A constitutive model and data for metals subjected to large strains, high strain rates and high temperatures, in: Proceedings of the Seventh International Symposium on Ballistics. The Netherlands, The Hague, pp 541–547
38. Wang Y, Zhou Y, Xia Y (2004) A constitutive description of tensile behavior for brass over a wide range of strain rates. Mat Sci Eng A-Struct 372:186–190
39. Takuda H, Mori K, Hatta N (1999) The application of some criteria for ductile fracture to the prediction of the forming limit of sheet metals. J Mater Process Tech 95:116–121
40. Faura F, Garcıia A, Estrems M (1998) Finite element analysis of optimum clearance in the blanking process. J Mater Process Tech 98:121–125
41. Cockroft MG, Latham DJ (1968) Ductility and workability of metals. J Inst Met 96:33–39
42. Velásquez JDP, Tidu A, Bolle B, Chevrier P, Fundenberger JJ (2010) Sub-surface and surface analysis of high speed machined Ti–6Al–4V alloy. Mat Sci Eng A-Struct 527:2572–2578
43. Che-Haron CH (2001) Tool life and surface integrity in turning titanium alloy. J Mater Process Tech 118:231–237
44. Ge YF, Xu JH, Yang H (2008) Workpiece surface quality when ultra-precision turning of SiCp/Al composites. J Mater Process Tech 203:166–175
45. Chou YK, Evans CJ (1999) White layers and thermal modeling of hard turned surfaces. Int J Mach Tool Manuf 39:1863–1881
46. Lee WS, Lin CF (1998) Plastic deformation and fracture behaviour of Ti–6Al–4V alloy loaded with high strain rate under various temperatures. Mater Sci Eng A-Struct 241:48–59